Electronic Supplementary Information

Self-templating Synthesis of Hollow Spheres of MOFs and Their Derived Nanostructures

*Ying Chuan Tan and Hua Chun Zeng**

Department of Chemical and Biomolecular Engineering, Faculty of Engineering, National University of Singapore, 10 Kent Ridge Crescent, Singapore 119260

* Email: chezhc@nus.edu.sg

Contents

Experimental Section

Materials. The following chemicals were used as received without further purification. Methanol (VWR Chemicals, analytical reagent grade), ethanol (VWR Chemicals, analytical reagent grade), dimethylformamide (DMF, VWR Chemicals, analytical reagent grade), 2-methylimidazole (HmIM, Aldrich, 99%), hexadecyltrimethylammonium bromide (C_{16}TAB, Fluka, >96.0%), tetradecyltrimethylammonium bromide (C_{14}TAB, Sigma, 99%), dodecyltrimethylammonium bromide (C_{12}TAB, Sigma, 99%), cobalt (II) nitrate hexahydrate ($Co(NO_3)_2 \cdot 6H_2O$, Sigma-Aldrich, ≥ 98%), copper (II) nitrate trihydrate ($Cu(NO_3)_2 \cdot 3H_2O$, Sigma-Aldrich, ≥ 98.0%), zinc (II) nitrate hexahydrate ($Zn(NO_3)_2 \cdot 6H_2O$, Sigma-Aldrich, 98%), tetraethyl orthosilicate (TEOS Aldrich, ≥99.0%), hexadecyltrimethylammonium chloride aqueous solution (C_{16}TAC, Aldrich, 25 wt.% in water), ammonia solution (Merck, 32%), ruthenium (IV) oxide (RuO_2, Aldrich, 99.9%), ultrapure water (Merck), perfluorosulfonic acid-PTFE copolymer (Nafion solution, Alfa Aesar, 5% w/w in water).

Synthesis of ZIF-67-HS. In general, 75 μL of aqueous 0.5 M $Co(NO_3)_2$ solution and 2 mL of aqueous 0.1 M C_{14}TAB solution were added to 12.6 mL of deionized water. This mixture was subsequently stirred for 5 min before instantaneous addition of 1.5 mL of aqueous 1.096 M HmIM solution. The reaction solution was left to stir continuously for 50 min. The product was then collected, centrifuged and washed for 4 cycles (first wash using DMF and subsequent washes using methanol) and later dried in an oven at 60 °C. The samples were dispersed in 2 mL methanol for further use (See Synthesis of ZIF-67@*m*SiO_2-HS and Co_3O_4@*m*SiO_2-HS).

Synthesis of M/ZIF-67-HS. Similar to the synthesis of ZIF-67-HS, 75 μL of aqueous 0.5 M $Co(NO_3)_2$ solution and 2 mL of aqueous 0.1 M C_{14}TAB solution were added to 12.6 mL of deionized water. This mixture was subsequently stirred for 5 min before instantaneous addition of 1.5 mL of aqueous 1.096 M HmIM solution. The reaction solution was left to stir for 20 min before 50 μL of aqueous 0.5 M $Cu(NO_3)_2$ solution or/and 0.5 M $Zn(NO_3)_2$ solution was added dropwise. The mixture was left to react for 30 min under stirring condition. The product was then collected, centrifuged and washed for 4 cycles (first wash using DMF and subsequent washes using methanol) and later dried in an oven at 60 °C.

Synthesis of Cu/ZIF-67-HS via Coprecipitation. Similar to the synthesis of ZIF-67-HS, 75 μL of aqueous 0.5 M $Co(NO_3)_2$ solution, 50 μL of aqueous 0.5 M $Cu(NO_3)_2$ solution and 2 mL of aqueous 0.1 M C_{14}TAB solution were added to 12.75 mL of deionized water. This mixture was subsequently stirred magnetically for 5 min before instantaneous addition of 1.3 mL of aqueous 1.096 M HmIM solution. The reaction solution was left to stir continuously for 90 min. The product was then collected, centrifuged and washed for 4 cycles (first wash using DMF and subsequent washes using methanol) and later dried in an oven at 60 °C.

Synthesis of ZIF-67-D. Briefly, 0.359 g of $Co(NO_3)_2$ was dissolved in 25mL of methanol, while 0.811 g of HmIM was dissolved in another 25 mL of methanol. These two methanolic solutions were mixed instantaneously together under rapid stirring for 1 min, and subsequently left to stand for 24 h. The product was then collected, centrifuged and washed for 4 cycles using methanol and later dried in an oven at 60 °C.

Synthesis of Co_3O_4-HS-1, M/Co_3O_4-HS-1 and Co_3O_4-D-1. The dried samples of ZIF-67-HS, M/ZIF-67-HS and ZIF-67-D were heated in an electric furnace at 260 °C in air for 3 h with a ramping rate of 2 °C min^{-1} to obtain Co_3O_4-HS-1, M/Co_3O_4-HS-1 and Co_3O_4-D-1 respectively.

Synthesis of Co_3O_4-HS-2, M/Co_3O_4-HS-2 and Co_3O_4-D-2. The dried samples of ZIF-67-HS, M/ZIF-67-HS and ZIF-67-D were heated in a tube furnace at 500 °C in 50 mL min^{-1} of Ar flow for 3 h with a ramping rate of 1 °C min^{-1}. Next, the cooled calcined samples were further heated in an electric furnace in air at 240 °C with a ramping rate of 2 °C min^{-1} to obtain Co_3O_4-HS-2, M/Co_3O_4-HS-2 and Co_3O_4-D-2 respectively.

Synthesis of Co-complex@ZIF-67-YS and Co/C-YS. Similar to the synthesis of ZIF-67-HS, once the products were collected, only 12 mL of DMF was used for washing, after which the samples were dried in an oven at 60 °C to obtain Co-complex@ZIF-67-YS. The dried sample was then heated in a tube furnace at 500 °C in 50 mL min^{-1} of Ar flow for 3 h with a ramping rate of 1 °C min^{-1}, thus yielding Co/C-YS.

Synthesis of ZIF-67@*m*SiO_2-HS and Co_3O_4@*m*SiO_2-HS. Following a method previously reported,[1] first, 33 mL deionized water, 21 mL methanol and 2.87 mL 1.096M HmIM solution were mixed homogeneously. After subsequent addition of 0.55 mL C_{16}TAC solution and 5 mL methanolic ZIF-67-HS suspension (see Synthesis of ZIF-67-HS), the mixture was ultrasonicated for 5 min and stirred for 20 min. Finally, 0.4 mL of TEOS was added dropwise over 3 min under stirring and the reaction mixture was continued to stir for another 1 h. The product was then collected, centrifuged and washed for 4 cycles using ethanol and later dried in an oven at 60 °C, thus obtaining ZIF-67@*m*SiO_2-HS. The powdered samples were then heated at 260 °C in air for 3 h with a ramping rate of 2 °C min^{-1} to produce Co_3O_4@*m*SiO_2-HS.

Synthesis of Stöber SiO_2. Using a modified Stöber method, 46 mL of ethanol was first mixed with 2.5 mL of TEOS and stirred for 15 min. Next, 5 mL of 25% ammonia solution was added instantaneously under vigorous stirring. The mixture was then stirred for another 3 h. The product was collected, centrifuged and washed for 3 cycles using ethanol and later dried in an oven at 60 °C.

Synthesis of SiO_2@ZIF-67-YS. Similar to the synthesis of ZIF-67-HS, 5 mg of Stöber SiO_2, 75 μL of aqueous 0.5 M $Co(NO_3)_2$ solution and 4 mL of aqueous 0.1 M C_{14}TAB solution were added to 10.1 mL of deionized water. This mixture was ultrasonicated for 5 min and stirred magnetically for 5 min before instantaneous addition of 1.8 mL of aqueous 1.096 M HmIM solution. The reaction solution was left to stir continuously for 50 min. The product was then collected, centrifuged and washed for 4 cycles (first wash using DMF and subsequent washes using methanol) and later dried in an oven at 60 °C.

Materials Characterization. The morphological features of the colloidal nanoparticles were investigated using transmission electron microscopy (TEM, JEM-2010, FETEM-2100F, accelerating voltage: 200 kV). The bulk morphology of samples was analyzed with scanning electron microscopy (FESEM, JEM-6700F, accelerating voltage: 15 kV, working distance: 15 mm). The crystallographic structure was determined by X-ray diffractometer (XRD, Bruker D8 Advance) equipped with Cu Kα radiation source. Specific surface area and pore size distribution of samples were obtained from N_2 physisorption isotherms at 77 K (Quantachrome NOVA-3000 system). Thermogravimetric analysis (TGA, Shimadzu, Model TGA-50) was also carried out in a purified air atmosphere (flow rate at 50 mL min^{-1}) at a heating rate of 2 °C min^{-1} from 30 °C to a holding temperature of 260 °C and heated for another 150 min. Metal content of catalyst was analyzed by inductively coupled plasma optical emission spectrometry (ICP-OES, Optima 7300DV, Perkin Elmer, USA).

Evaluation of the Electrocatalytic Performance toward OER. To prepare the catalyst ink, 5 mg of catalyst was added to 1.11 mL solution of 8:2:0.5 (v/v) mixture containing ultrapure water, ethanol and commercial Nafion solution, followed by ultrasonication for 30 min. By drop-casting 3 μL of the homogeneous catalyst ink onto a polished glassy carbon electrode (GCE, 3 mm in diameter), a total catalyst loading of ~0.2 mg $\mathrm{cm^{-1}}$ was achieved. The catalytic activity was evaluated using Autolab PGSTAT 302N potentiostat in a standard three-electrode system, consisting of a Ag/AgCl (in 3 M aqueous KCl) reference electrode, a platinum foil counter electrode and a GCE as a working electrode. An O_2-saturated 0.1 M KOH electrolyte was used for all electrochemical measurements. All of the potentials were referred to the reversible hydrogen electrode (RHE) with the following equation:

$$E(\mathrm{RHE}) = E(\mathrm{V\ vs\ Ag/AgCl/\ 3\ M\ KCl}) + 0.977$$

Cyclic voltammetry (CV) and linear sweep voltammetry (LSV) were carried out at a scan rate of 10 mV $\mathrm{s^{-1}}$. Before carrying out LSV measurements, CV was done for several cycles until a stable response was obtained. All of the polarization curves were 95% *iR* compensated. The relative electrochemical active surface area of the catalysts was estimated by determining their electrochemical double-layer capacitance (C_{dl}), which is linearly proportional to the effective surface area. C_{dl} (mF $\mathrm{cm^{-2}}$) was determined from the CV curves measured in a 0.1 V potential range without faradaic process at different scan rates according to the following equation:

$$J_c = C_{dl} \cdot v$$

where J_c and v are the capacitive current density (mA $\mathrm{cm^{-2}}$) and scan rate (V $\mathrm{s^{-1}}$). By plotting the average capacitive current density at the open circuit potential against the scan rate, the measured slope of the plot represents the C_{dl}.

Supplementary Figures, Schemes, and Tables

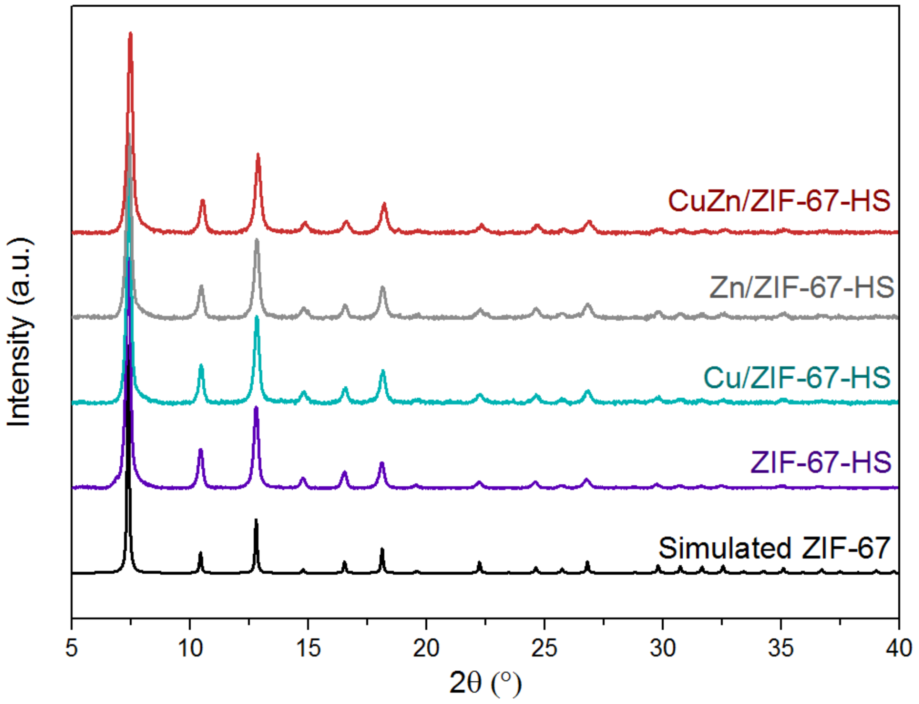

Figure S1. PXRD patterns of ZIF-67-HS and its various metal-doped M/ZIF-67-HS.

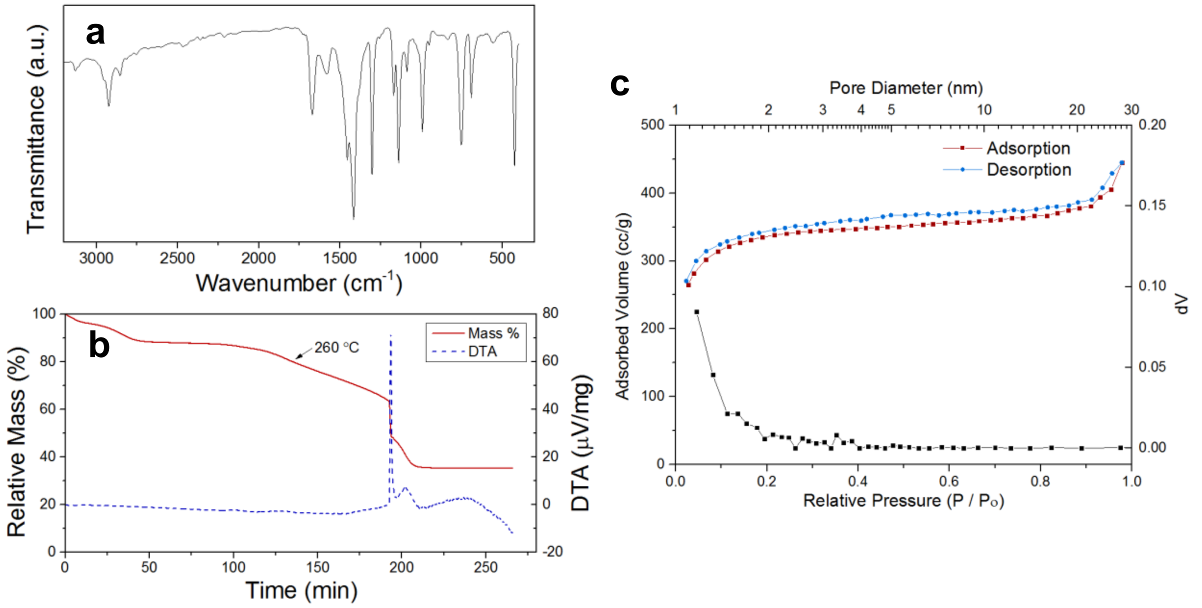

Figure S2. (a) FTIR spectrum of as-synthesized ZIF-67-HS, (b) TGA-DTA curves of ZIF-67-HS in air with a ramping rate of 2 °C·min^{-1} to a holding temperature of 260 °C and (c) nitrogen adsorption-desorption isotherms and BJH pore size distribution of ZIF-67-HS.

Presence of C_{14}TAB

Due to the usage of C_{14}TAB, residual surfactant molecules are expected to be present even after thorough washing. This is evident from the Fourier Transform Infrared (FT-IR) spectra presented in Figure S2a, in which the peaks of symmetric and asymmetric stretching modes of CH_2 are observed at 2855 cm^{-1} and 2924 cm^{-1} respectively. Similarly, from the thermogravimetric (TG) curve obtained for ZIF-67-HS in Figure S2b, the two distinct exothermic peaks that occurred during the sudden loss of sample mass indicated a two-step decomposition; the first possibly attributed to the oxidation of C_{14}TAB present, while the second was due to the oxidation of the organic linkers within the ZIF-67.

Table S1. List of reported BET surface area and pore volume of ZIF-67 via aqueous synthesis.

Conditions	BET ($m^2\ g^{-1}$)	Pore Volume ($cc\ g^{-1}$)	Ref.
Room temperature with C_{14}TAB	1308	0.50	*This work*
Room temperature with TEA	663	-	2
Room temperature with TEA	868	0.38	3
Room temperature with TEA	601	-	4
Room temperature	316	0.17	5
Room temperature	621.4	-	6
Room temperature with NH_4OH & P123	869	-	7
Room temperature with NH_4OH, Pluronic F127 & CTAB	1103	0.34	8
Room temperature with NH_4OH & Pluronic F127	1710	0.42	
Room temperature	734	0.34	9

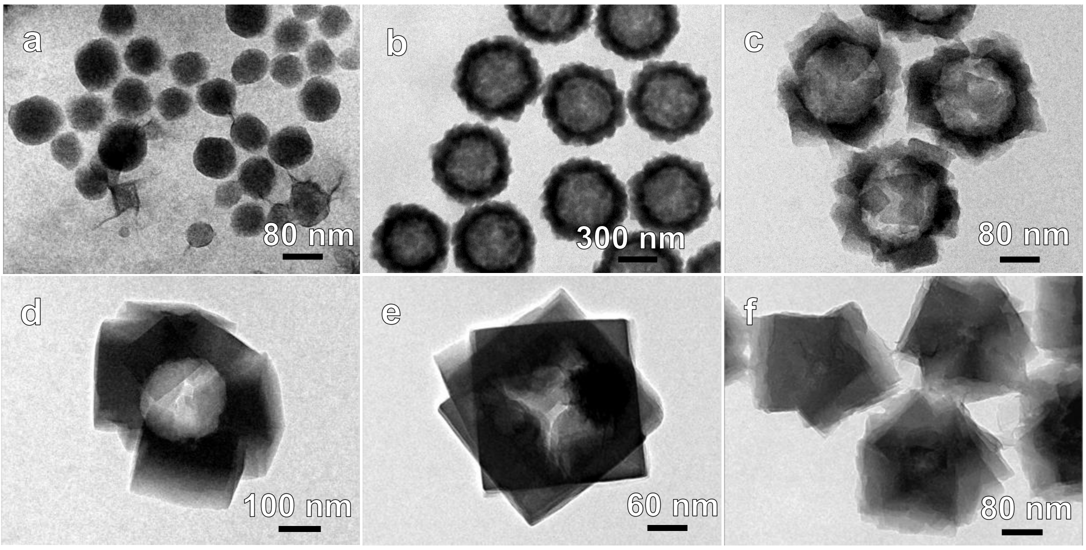

Figure S3. TEM images of products obtained by varying the amount precursor used (see Synthesis of ZIF-67-HS) while keeping the total mixture volume constant: (a) no C_{14}TAB added, (b) C_{14}TAB replaced with C_{16}TAB with reaction time of 4 h, (c) C_{14}TAB replaced with C_{12}TAB with reaction time of 40 min, (d) 40 μL of 0.5 M $Co(NO_3)_2$ and 1.3 mL of 1.096 M HmIM used, (e) 50 μL of 0.5 M $Co(NO_3)_2$ and 1.2 mL of 1.096 M HmIM used and (f) 1.3 mL of 1.096 M HmIM used.

Table S2. Mean diameter of as-synthesized ZIF-67-HS by varying the surfactant used and the volume of aqueous 0.5 M $Co(NO_3)_2$ added.

Surfactant	Volume of $Co(NO_3)_2$ added		
	50 μL	75 μL	100 μL
C_{12}TAB	302 nm	225 nm	-
C_{14}TAB	357 nm	325 nm	248 nm
C_{16}TAB	625 nm	523 nm	390 nm

Effect of synthesis parameters

Synthesis parameters in this approach play a crucial role in the morphology control of ZIF-67-HS. The effects of the surfactant used are shown in Figure S3a–c. In the absence of C_{14}TAB, spherical ZIF-67 particles (smaller than 100 nm) and sheet-like hydroxide side-products were formed. Moreover, when the length of carbon chain in C_nTAB used was varied, the mean diameter of the ZIF-67-HS produced was changed as well. Micelles formed in aqueous C_nTAB solution were reported to increase in size as the length of the carbon chain increased.[10] When $[Co^{2+}]$ was adjusted, the size of ZIF-67-HS was also altered to a smaller extent, which suggested that the diameter of vesicle was also affected by the amount of $Co(NO_3)_2$ added. By controlling both surfactant and Co^{2+}, the dimension of ZIF-67-HS can be tuned within 225−625 nm as summarized in Table S2.

In general, when the concentrations of precursors are lowered, the number of nucleation spots decreases and thus crystals tend to grow larger in size. This trend was also observed for the synthesis of ZIF-67-HS. As the volumes of $Co(NO_3)_2$ and HmIM solutions added were decreased, the individual size of ZIF-67 crystals increased with a more apparent cubic structure on the exterior, while the hollow spherical interior of the overall particle was retained (See Figure S3d). On the other hand, if the amount of Co^{2+} ions was reduced to a lesser extent compared to HmIM, the hollow core appeared to be less spherical (see Figure S3e), indicating a growth towards the inner core. Lastly, when only HmIM amount was lowered, the inner void became even less apparent as shown in Figure S3f. From the above observations, as the metal to ligand ratio increases, it is possible that the HmIM in the bulk solution gets consumed up first to form a preliminary hollow ZIF-67 structure, after which the HmIM source in the core lipid soft template is used for further crystal growth due to the presence of excess Co^{2+} ions in the bulk solution that diffuse through the MOF shell.

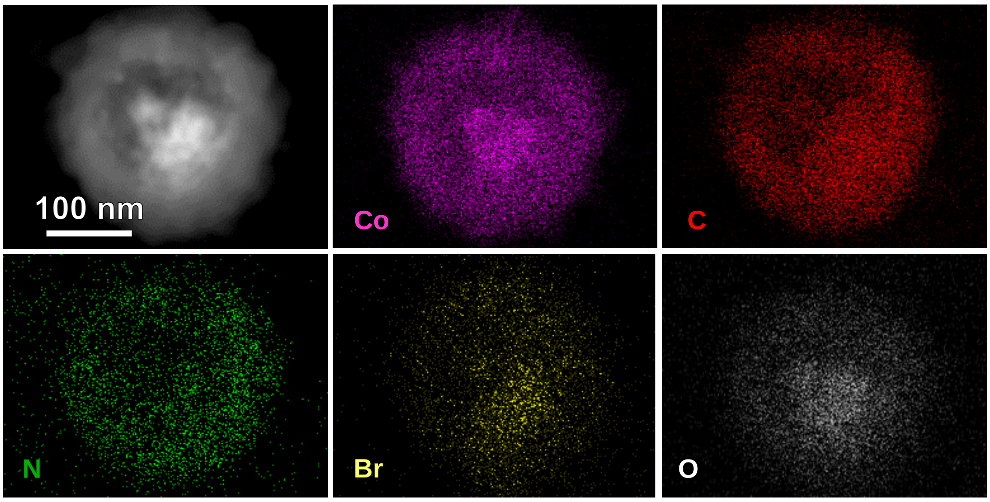

Figure S4. HAADF-STEM image of unwashed ZIF-67-HS and its corresponding EDX elemental mappings.

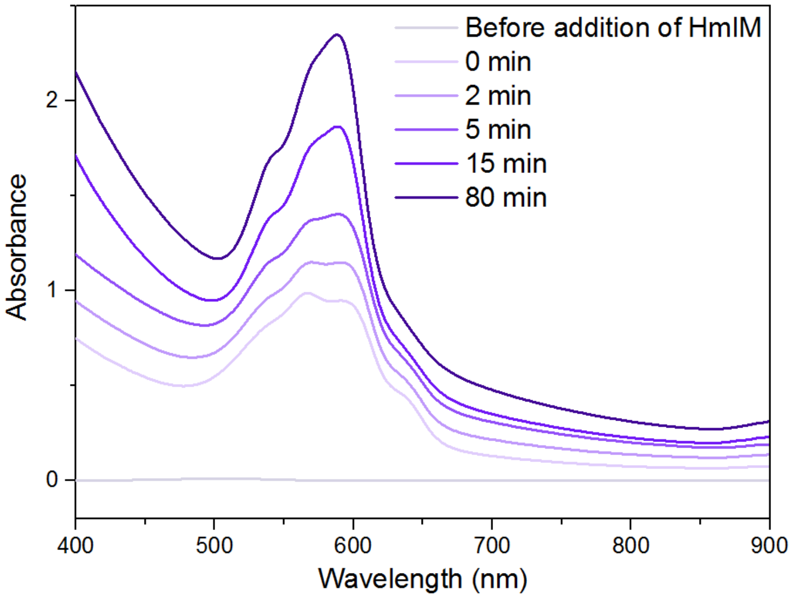

Figure S5. Evolution of UV-Vis spectra of the reaction mixture over time.

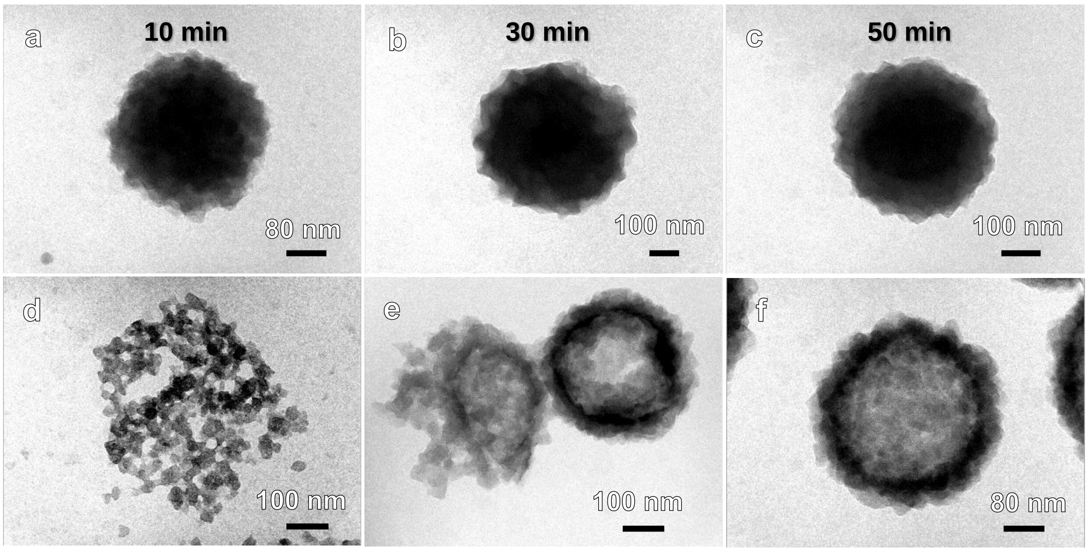

Figure S6. TEM images obtained at different synthesis time intervals of the ZIF-67-HS samples (a–c) before washing and (d–f) after washing.

As presented in Figure S6a–c, before each sample was washed at every time interval, the vesicle@ZIF-67 composites existed as sub-micron spheres, which were similar to the illustrations in Scheme 1b,c. Due to the unwashed residues present in the samples, amorphous materials were observed on the surface of the spheres.

With adequate washing using organic solvents, the vesicular templates were removed. When the synthesis was stopped after 10 min, the ZIF-67 crystals (~30 nm) were observed to be loosely packed without any 3-dimensional assembled structure (Figure S6d). At this stage, nucleation and island formation of ZIF-67 crystals had just occurred and the connectivity between crystals was low (Scheme 1b). Therefore, once the soft template was removed, the spherical structure collapsed and resulted in a 2-dimensional porous aggregate of ZIF-67 nanocrystals. As the synthesis time was extended to 30 min, partial spherical assemblies of ZIF-67 nanocrystals were observed (Figure S6e), which suggested a higher level of coalescence between crystals as the growth proceeded. Finally, a complete formation of ZIF-67-HS was evident after 50 min of reaction time (Figure S6f).

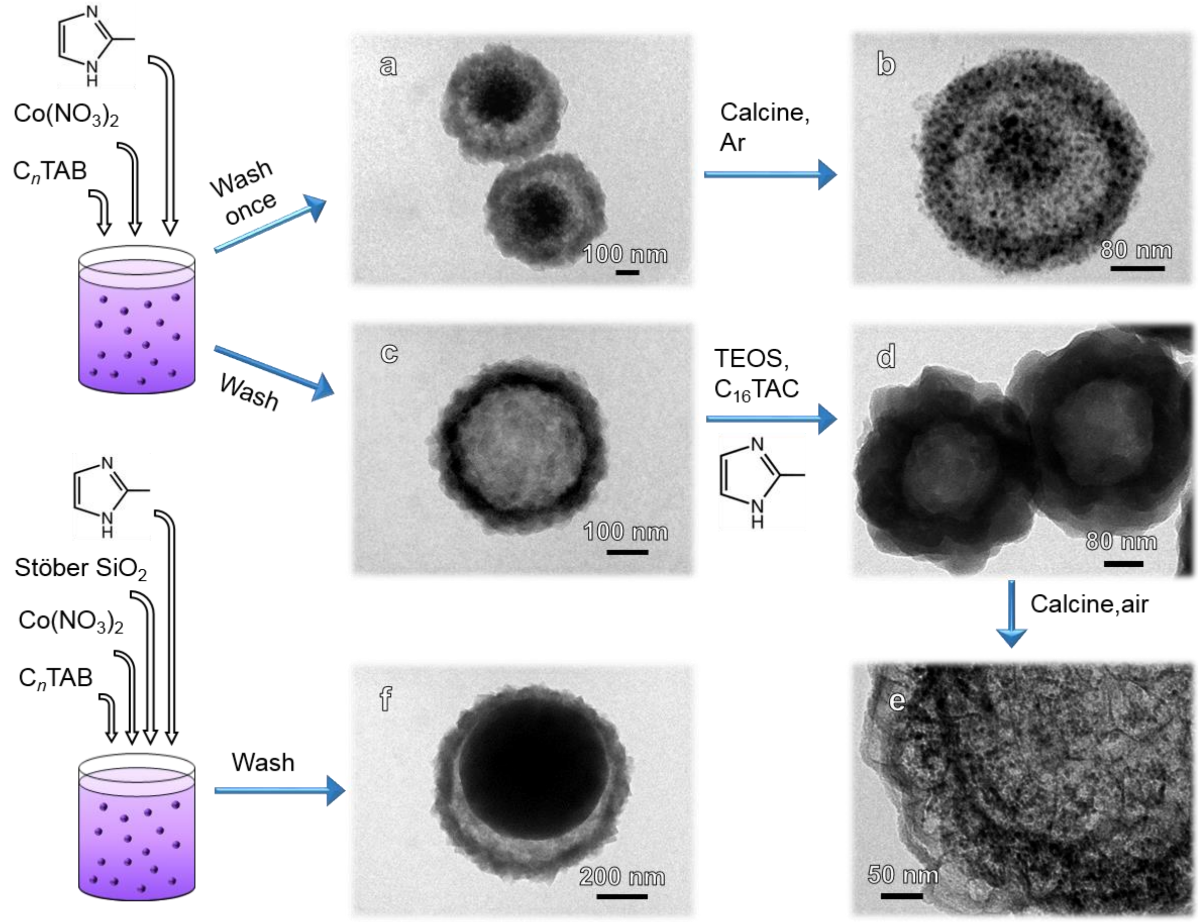

Scheme S1. Stepwise synthetic method for designing of ZIF-67-integrated nanocomposites and their derived nanostructures: (a) Co-complex@ZIF-67-YS, (b) Co/C-YS, (c) ZIF-67-HS, (d) ZIF-67@*m*SiO$_2$-HS, (e) Co$_3$O$_4$@*m*SiO$_2$-HS and (f) SiO$_2$@ZIF-67-YS.

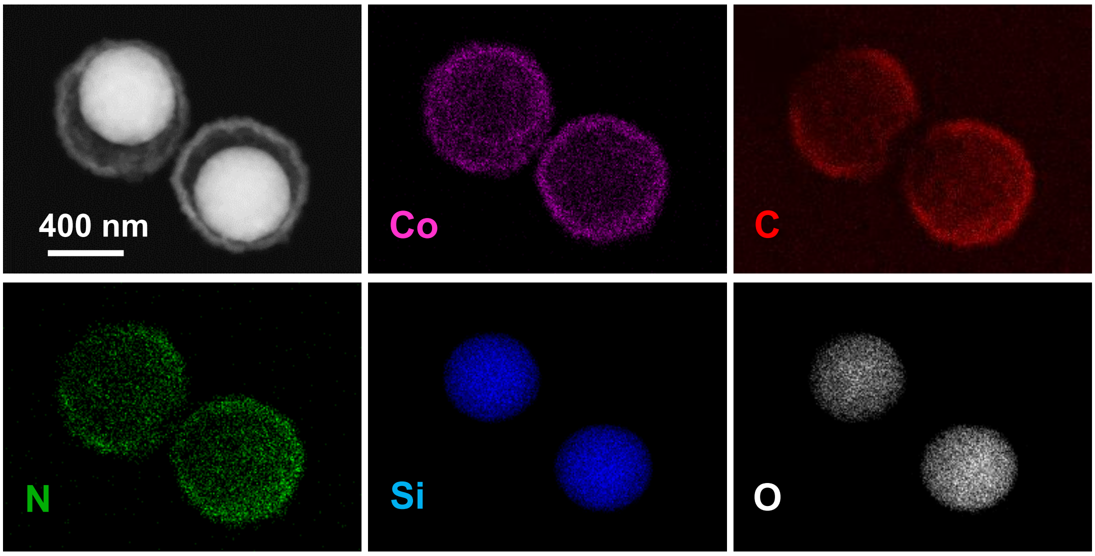

Figure S7. HAADF-STEM image, and the corresponding EDX elemental mapping images of SiO$_2$@ZIF-67-YS.

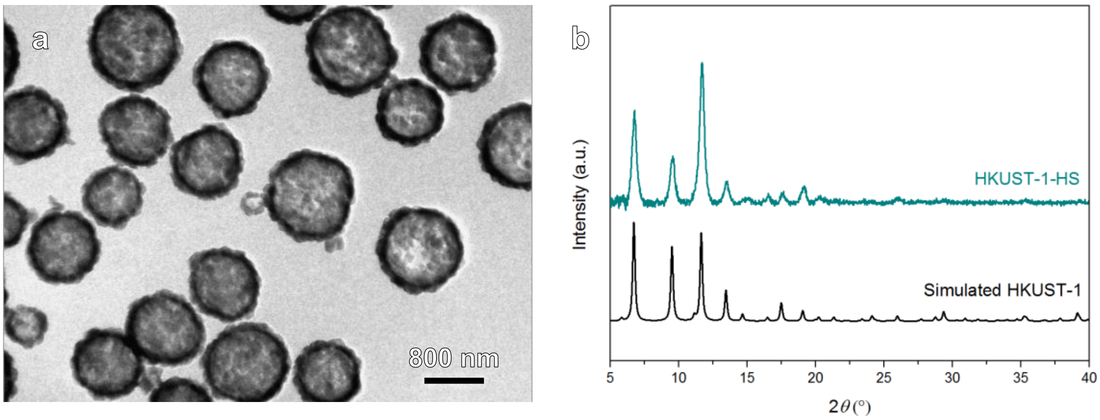

Figure S8. (a) TEM image of HKUST-1-HS and (b) PXRD pattern of as-synthesized HKUST-1-HS.

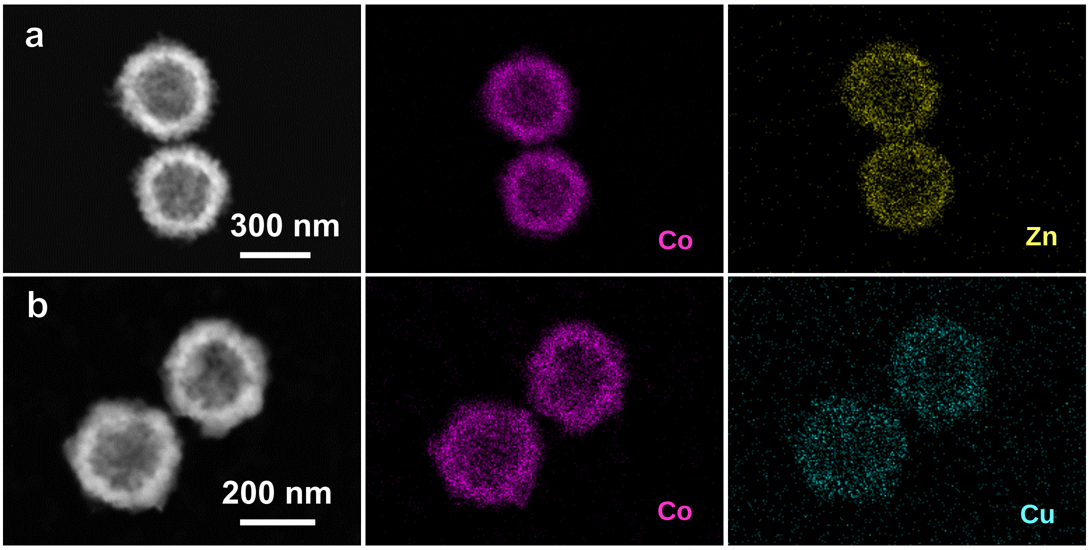

Figure S9. HAADF-STEM images of (a) Zn/ZIF-67-HS and (b) Cu/ZIF-67-HS and their corresponding EDX metallic elemental mapping images.

Table S3. Summary of the metal compositions in the as-synthesized M/ZIF-67-HS.

Sample	Co (mol %)	Cu (mol %)	Zn (mol %)
Cu/ZIF-67-HS[a]	76.5	23.5	-
Cu/ZIF-67-HS-low	93.1	6.9	-
Zn/ZIF-67-HS	87.3	-	12.7
CuZn/ZIF-67-HS	84.0	3.9	12.1

[a] To obtain a higher Cu to Co ratio, coprecipitation method was used (refer to Synthesis of Cu/ZIF-67-HS via Coprecipitation in Experimental Section).

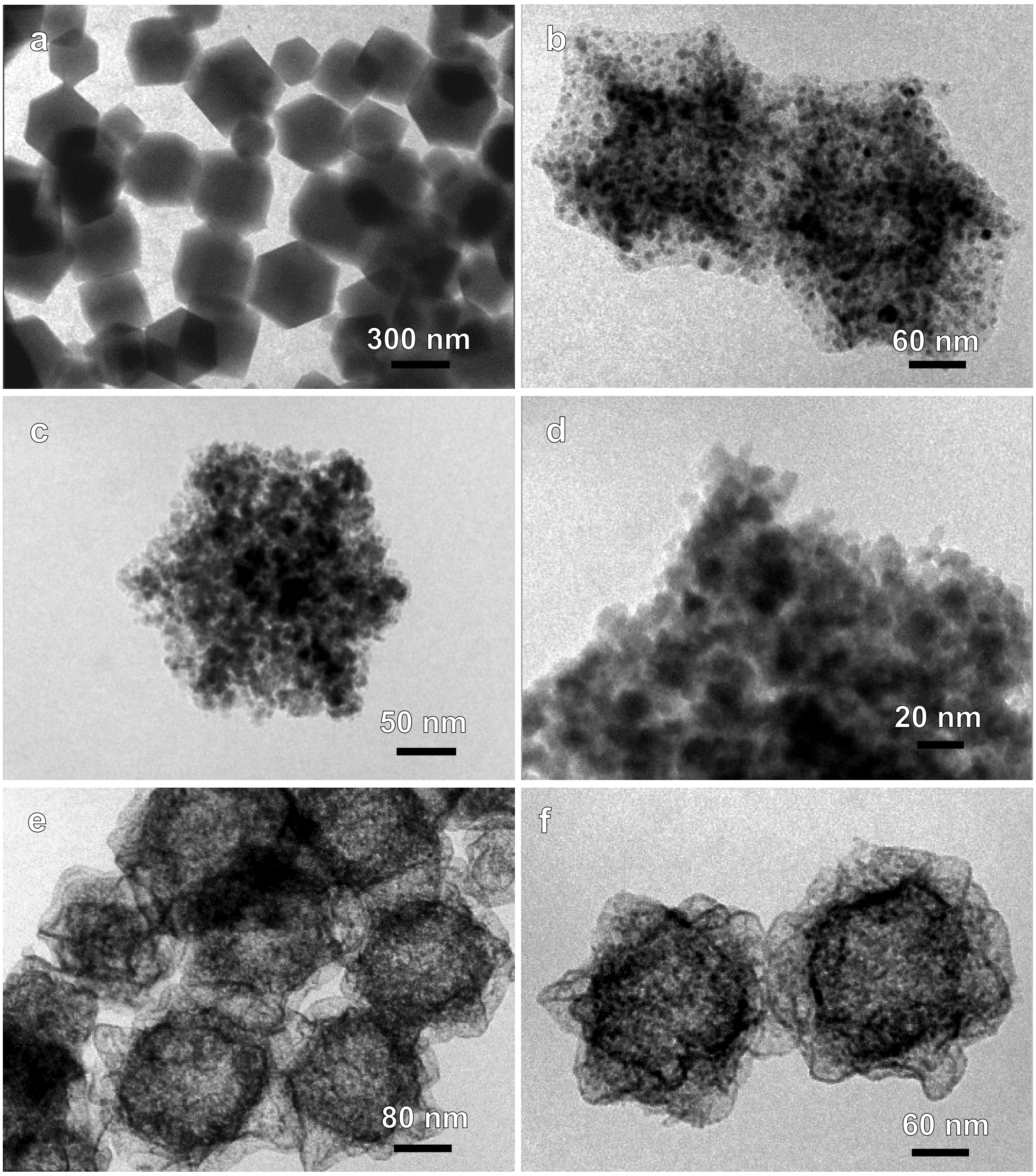

Figure S10. TEM images of (a) ZIF-67-D and the corresponding products under different calcination treatment: (b) 500 °C for 3h at a ramping rate of 1 °C/min in argon, (c,d) 500 °C for 3h at a ramping rate of 1 °C/min in argon, followed by 240 °C at a ramping rate of 2 °C/min in air, yielding Co_3O_4-D-2 and (e,f) 260 °C for 3h at a ramping rate of 2 °C/min in air, yielding Co_3O_4-D-1.

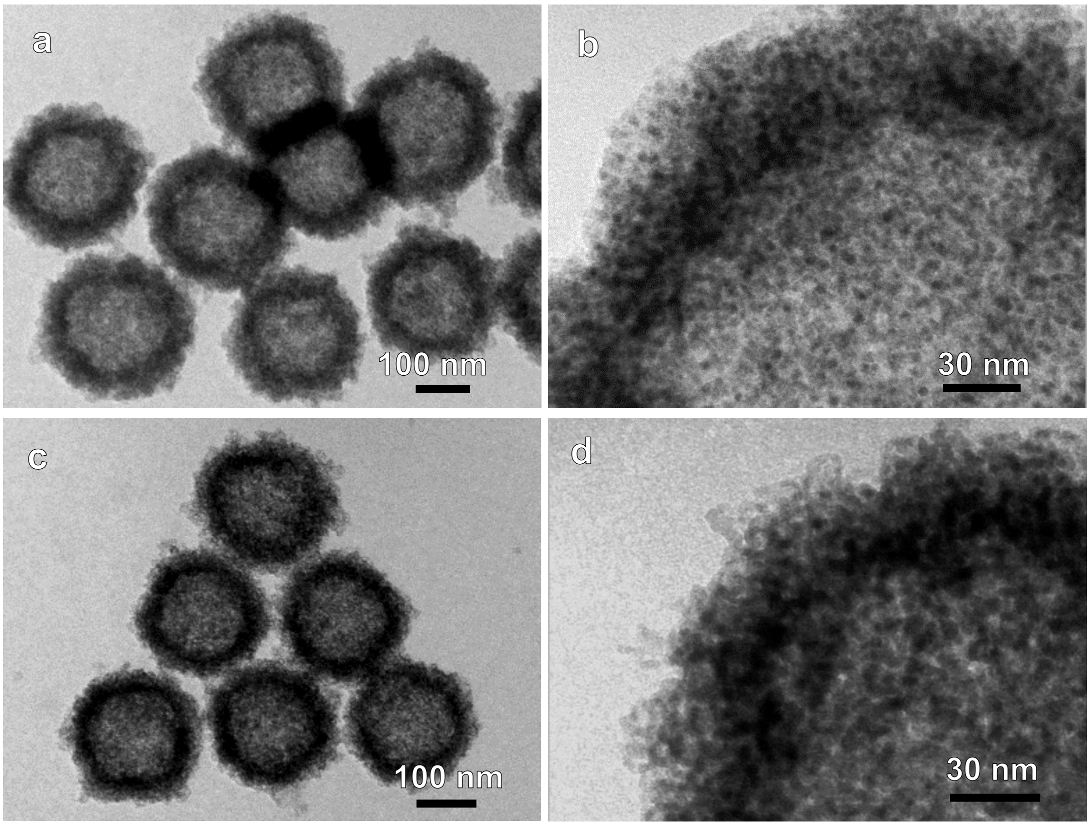

Figure S11. TEM images (at different magnifications) of ZIF-67-HS after different calcination treatment: (a,b) 500 °C for 3h at a ramping rate of 1 °C/min in argon, and (c,d) 260 °C for 3h at a ramping rate of 2 °C/min in air, ZIF-67-HS-1.

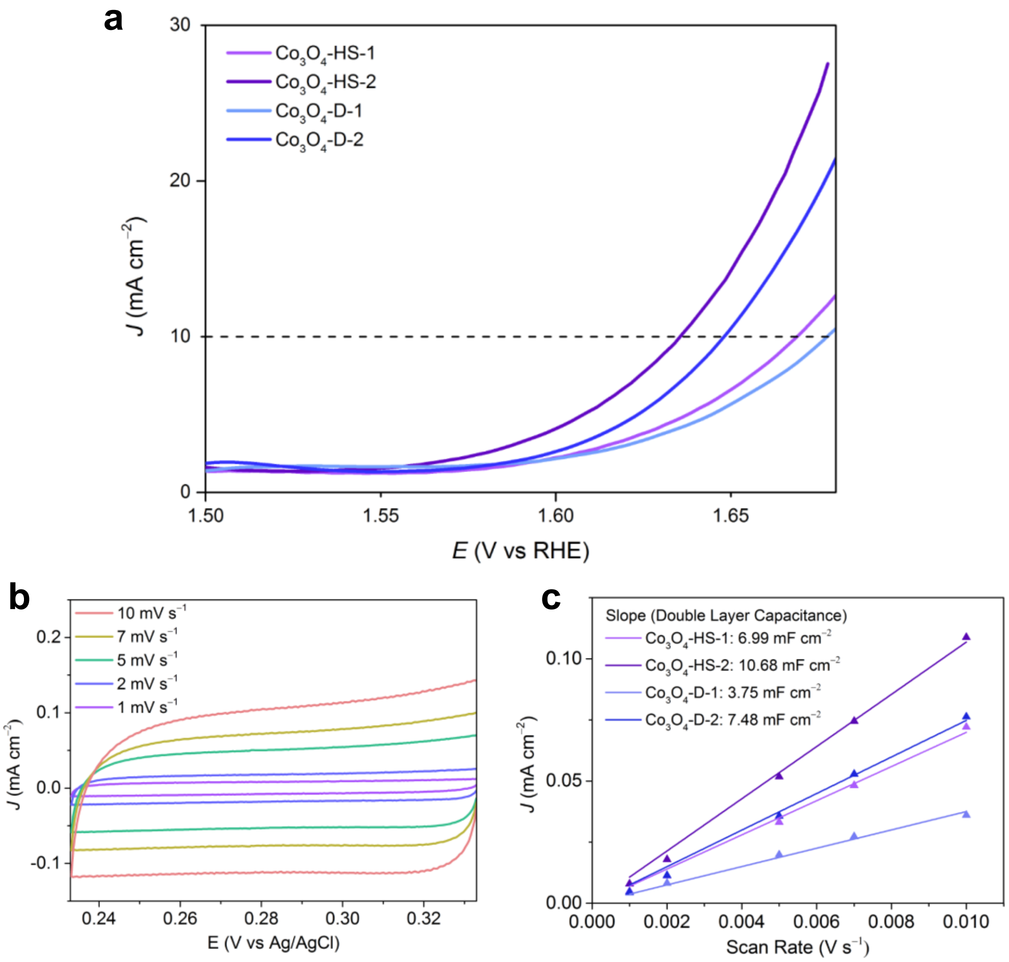

Figure S12. (a) LSV measurements of Co_3O_4 products using different ZIF-67 templates and thermal treatments, (b) cyclic voltammograms of Co_3O_4-HS-2 in a 0.1 V potential window without faradaic process at different scan rates, (c) average capacitive current densities of the different Co_3O_4 products the open-circuit potential for the measured scan rates and their corresponding double layer capacitances. Data interpretation in the plots of (c) can be referred to Experimental Section (Electronic Supporting Information).

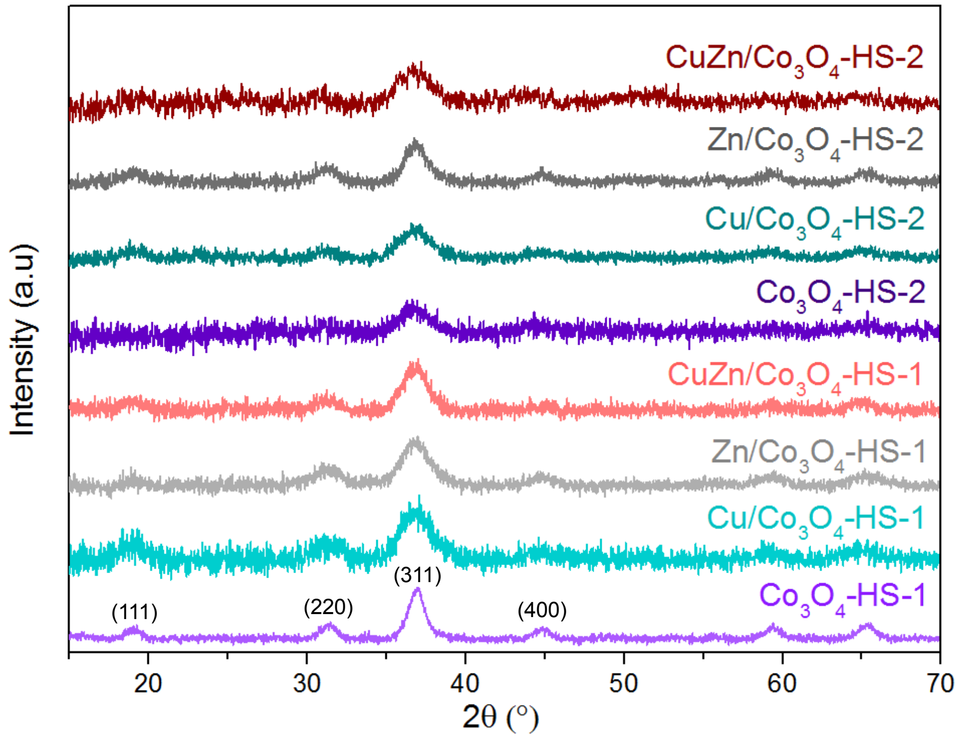

Figure S13. PXRD patterns of Co_3O_4-HS and its various metal-doped M/Co_3O_4-HS under two different thermal treatment conditions, of which all calcined samples are consistent with the standard XRD patterns of cubic spinel Co-based oxides (JCPDS File No. 42-1467).

Table S4. List of reported Co_3O_4 and cobalt oxide-based nanomaterials used for OER and their respective activities.

Materials	Overpotential (mV) at 10 mA cm^{-1}	Catalyst Loading (mg cm^{-1})	Electrolyte	Substrate	Ref.
Co_3O_4-HS-2	405	0.2	0.1 M KOH	GCE	*This work*
Co_3O_4	525	0.13	0.1 M KOH	GCE	11
Co_3O_4	450	0.35	0.1 M KOH	GCE	12
Co_3O_4	523	0.56	0.1 M KOH	GCE	13
Co_3O_4	409	0.14	1 M KOH	GCE	14
Co_3O_4	380	0.2	1 M KOH	GCE	15
Co_3O_4	410	1.0	1 M KOH	Ni foam	16
Cu/Co_3O_4-HS-2[b]	361	0.2	0.1 M KOH	GCE	*This work*
Co@C/N-doped graphene	430	0.36	0.1 M KOH	GCE	17
Co_3O_4/C nanoarray	290	0.2	0.1 M KOH	Cu foil	18
Co_3O_4/C	360	0.28	0.1 M KOH	GCE	19
Co_3O_4/graphene	359	0.2	0.1 M KOH	GCE	20
Co/C	390	0.2	0.1 M KOH	GCE	21
Au@Co_3O_4	380	0.2	0.1 M KOH	GCE	22
$Zn_xCo_{3-x}O_4$ nanoarray	320	1.0	1 M KOH	Ti foil	23
Co_3O_4/$NiCo_2O_4$	340	1.0	1 M KOH	Ni foam	16
CoO_x/N-doped C	410 / 385 (after running HER)	0.42	1 M KOH	GCE	24

[b] More specifically in spinel oxide phase $Cu_{0.7}Co_{2.3}O_4$.

References

1. Z. Li and H. C. Zeng, *J. Am. Chem. Soc.*, 2014, **136**, 5631-5639.
2. G. Yu, J. Sun, F. Muhammad, P. Wang and G. Zhu, *RSC Advances*, 2014, **4**, 38804.
3. A. F. Gross, E. Sherman and J. J. Vajo, *Dalton transactions*, 2012, **41**, 5458-5460.
4. T. Truong, T. M. Hoang, C. K. Nguyen, Q. T. N. Huynh and N. T. S. Phan, *RSC Adv.*, 2015, **5**, 24769-24776.
5. J. Qian, F. Sun and L. Qin, *Mater. Lett.*, 2012, **82**, 220-223.
6. Y. Gao, J. Wu, W. Zhang, Y. Tan, J. Gao, J. Zhao and B. Tang, *New J. Chem.*, 2015, **39**, 94-97.
7. J. Yao, M. He, K. Wang, R. Chen, Z. Zhong and H. Wang, *CrystEngComm*, 2013, **15**, 3601.
8. K.-Y. Andrew Lin, H. Yang and W.-D. Lee, *RSC Adv.*, 2015, **5**, 81330-81340.
9. X. Guo, T. Xing, Y. Lou and J. Chen, *J. Solid State Chem.*, 2016, **235**, 107-112.
10. S. Berr, R. R. Jones and J. S. Johnson Jr, *J. Phys. Chem.*, 1992, **96**, 5611-5614.
11. H. Tüysüz, Y. J. Hwang, S. B. Khan, A. M. Asiri and P. Yang, *Nano Research*, 2012, **6**, 47-54.
12. L. Li, T. Tian, J. Jiang and L. Ai, *J. Power Sources*, 2015, **294**, 103-111.
13. X. Zhou, Z. Xia, Z. Tian and Y. Ma, Y. Qu, *J. Mater. Chem.*, *A* 2015, **3**, 8107-8114.
14. X. Zhou, X. Shen, Z. Xia, Z. Zhang, J. Li, Y. Ma and Y. Qu, *ACS Appl. Mater. Interfaces*, 2015, **7**, 20322-20331.
15. S. Chen, Y. Zhao, B. Sun, Z. Ao, X. Xie, Y. Wei and G. Wang, *ACS Appl. Mater. Interfaces*, 2015, **7**, 3306-3313.
16. H. Hu, B. Guan, B. Xia and X. W. Lou, *J. Am. Chem. Soc.*, 2015, **137**, 5590-5595.
17. Y. Hou, Z. Wen, S. Cui, S. Ci and S. Mao, J. Chen, *Adv. Funct. Mater.*, 2015, **25**, 872-882.
18. T. Y. Ma, S. Dai, M. Jaroniec and S. Z. Qiao, *J. Am. Chem. Soc.*, 2014, **136**, 13925-13931.
19. C. Zhang, M. Antonietti and T.-P. Fellinger, *Adv. Funct. Mater.*, 2014, **24**, 7655-7665.
20. Y. Zhao, S. Chen, B. Sun, D. Su, X. Huang, H. Liu, Y. Yan, K. Sun and G. Wang, *Sci. Rep.*, 2015, **5**, 7629.
21. L. Wu, Q. Li, C. H. Wu, H. Zhu, A. Mendoza-Garcia, B. Shen, J. Guo and S. Sun, *J. Am. Chem. Soc.*, 2015, **137**, 7071-7074.
22. Z. Zhuang, W. Sheng and Y. Yan, *Adv. Mater.*, 2014, **26**, 3950-3955.
23. X. Liu, Z. Chang, L. Luo, T. Xu, X. Lei, J. Liu and X. Sun, *Chem. Mater.*, 2014, **26**, 1889-1895.
24. H. Jin, J. Wang, D. Su, Z. Wei, Z. Pang and Y. Wang, *J. Am. Chem. Soc.*, 2015, **137**, 2688-2694.